Geophysical Research Letters

RESEARCH LETTER
10.1029/2021GL094966

Key Points:

- Ultrawide band microwave radar reveals spatially highly variable surface mass balance (SMB) over the past three centuries in inland Antarctica
- SMB anomalies resulting from local surface slopes may represent as much as 8–10% of the total SMB on the inland plateau
- The new SMB data have direct implications for the search for million-year-old ice in the Dome Fuji area, East Antarctica

Supporting Information:

Supporting Information may be found in the online version of this article.

Correspondence to:

B. Van Liefferinge,
bvlieffe@gmail.com

Citation:

Van Liefferinge, B., Taylor, D., Tsutaki, S., Fujita, S., Gogineni, P., Kawamura, K., et al. (2021). Surface mass balance controlled by local surface slope in inland Antarctica: Implications for ice-sheet mass balance and Oldest Ice delineation in Dome Fuji. *Geophysical Research Letters*, *48*, e2021GL094966. https://doi.org/10.1029/2021GL094966

Received 10 AUG 2021
Accepted 30 NOV 2021

Surface Mass Balance Controlled by Local Surface Slope in Inland Antarctica: Implications for Ice-Sheet Mass Balance and Oldest Ice Delineation in Dome Fuji

Brice Van Liefferinge[1], Drew Taylor[2], Shun Tsutaki[3], Shuji Fujita[3,4], Prasad Gogineni[2], Kenji Kawamura[3,4,5], Kenichi Matsuoka[1], Geir Moholdt[1], Ikumi Oyabu[3], Ayako Abe-Ouchi[6], Abhishek Awasthi[2], Christo Buizert[7], Jean-Charles Gallet[1], Elisabeth Isaksson[1], Hideaki Motoyama[3,4], Fumio Nakazawa[3,4], Hiroshi Ohno[8], Charles O'Neill[2], Frank Pattyn[9], and Konosuke Sugiura[10]

[1]Norwegian Polar Institute, Troms, Norway, [2]Remote Sensing Center, The University of Alabama, Tuscaloosa, AL, USA, [3]National Institute of Polar Research, Research Organization of Information and Systems (ROIS), Tokyo, Japan, [4]Department of Polar Science, The Graduate University of Advanced Studies (SOKENDAI), Tokyo, Japan, [5]Japan Agency for Marine Science and Technology (JAMSTEC), Yokosuka, Japan, [6]Atmosphere and Ocean Research Institute, The University of Tokyo, Kashiwa, Japan, [7]College of Earth, Ocean, and Atmospheric Sciences, Oregon State University, Corvallis, OR, USA, [8]Department of Civil and Environmental Engineering, Kitami Institute of Technology, Kitami, Japan, [9]Laboratoire de Glaciologie, Université libre de Bruxelles, Brussels, Belgium, [10]University of Toyama, Toyama, Japan

Abstract The limited number of surface mass balance (SMB) observations in the Antarctic inland hampers estimates of ice-sheet contribution to global sea level and locations with million-year-old ice. We present finely resolved SMB over the past three centuries in a low-accumulation region with significant depth hoar formation on Dome Fuji derived from ∼1,100 km of microwave radar stratigraphy dated with a firn core. The regional-mean SMB over the past 264 years is estimated to ∼22.5 ± 3.3 kg m^{-2} a^{-1}, but with large local variability of up to 30%. We found that local SMB is negatively correlated with surface slope at scales of a few hundred meters, resulting in anomalous zones of low SMB which represent as much as 8–10% of the total SMB on the inland plateau if the SMB-slope relationship is more widely valid. This impact should be investigated further to improve estimates of Antarctic mass balance and sea-level contribution.

Plain Language Summary Sampling the world's Oldest Ice (more than 1 million years) is crucial for understanding why pacing of glacier-interglacial cycles has changed in the past. Such ice will be preserved at the base of the Antarctic ice-sheet interior, though its location depends on many factors, including snow accumulation rate. We mapped snow accumulation in the Dome Fuji region, using radar-detected snow layers dated with volcanic signals in ice cores. Although climate models indicate a very low and nearly uniform snow accumulation in this region, the observations show large variations of up to about 30% which we found to be related to local surface slope at a scale of a kilometer or less. This new knowledge contributes to better locate Oldest Ice and to improve estimates of ice-sheet mass changes and its contributions to global sea level.

1. Introduction

The surface mass balance (SMB) of the Antarctic ice sheet has a strong gradient from the coast to inland, and is determined by complicated interactions between the atmosphere and the landscape. Satellite observations, regional climate models, and global circulation models typically resolve SMB distribution with a spatial resolution of tens of kilometers, which is not adequate to detect local features in SMB even in inland Antarctica where the surface topography is relatively smooth (e.g., Das et al., 2013). Microwave radar surveys of shallow firn stratigraphy and associated firn core analysis are viable means to address how these local features impact SMB at different spatial scales.

Detailed knowledge of SMB distribution is also important for selecting suitable ice coring sites, assuming that such patterns persist over time. Areas around Dome Fuji, Dome C, and a few other locations in East Antarctica have been suggested as promising sites to retrieve records of "Oldest Ice," which covers the mid-Pleistocene climate transition (Fischer et al., 2013), while the currently continuous ice core records are limited to the last 800 ka at Dome C (Jouzel et al., 2007). The likelihood of frozen bed and very old ice near the base generally increases

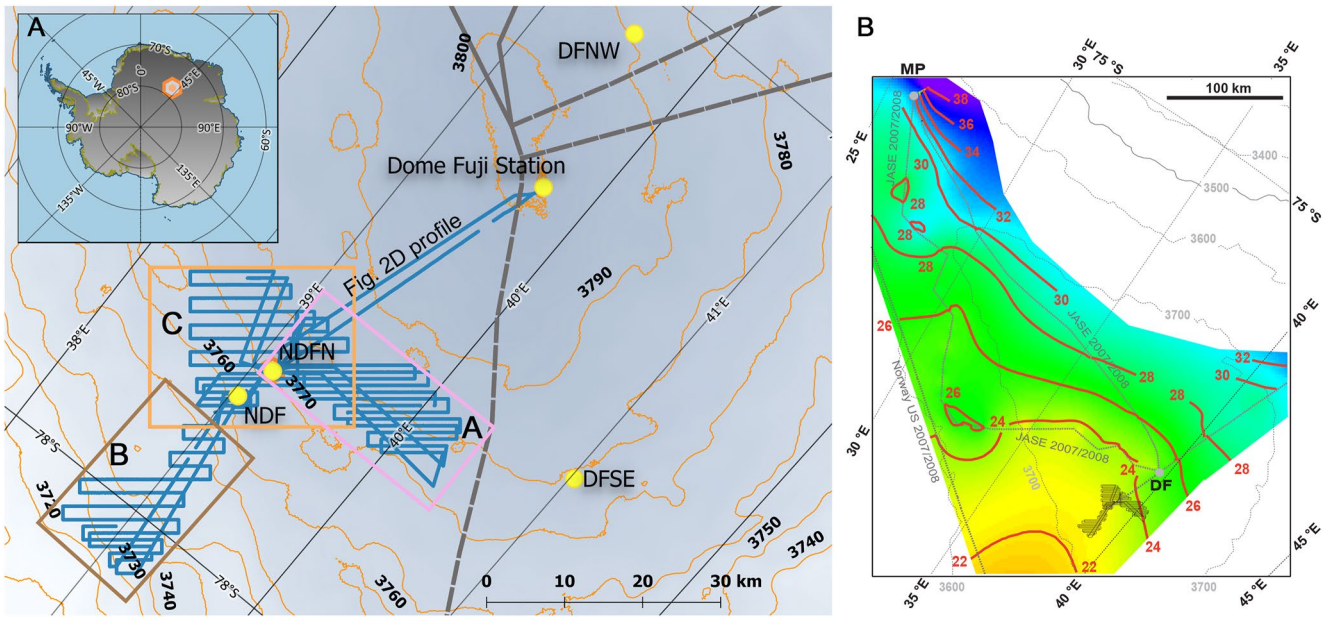

Figure 1. The Dome Fuji region, East Antarctica. (a) Radar data analyzed in this study were collected along the blue segments in three boxes, A, B, and C and between NDFN and Dome Fuji Station. According to the Japanese and German bed topography data, Box A include smoother bed, Box B has relatively thick ice that gives frozen bed if geothermal heat flow is proportionately low, and Box C has elevated bed which may constrain the ice-dome position in the past. Boxes A and C are located on one side of the subglacial massif, and Box B is located on the other side. Contours show surface elevations with 10-m internals (Howat et al., 2019). Yellow dots show locations of the four firn cores drilled in the 2017–2018 and 2018–2019 seasons, and the Dome Fuji Station where deeper cores have been drilled in the past (see Table S2 for coordinates). The black dashed line depicts ice flow divides from the MEaSUREs data set (Mouginot et al., 2017). The inset in A shows the coverage of the main map. (b) Overview of the larger region with the radar survey grid shown together with past surface mass balance (SMB) traverse routes by Japan-Sweden (Fujita et al., 2011) and Norway-US (Müller et al., 2010). The background colors show interpolated large-scale SMB for the last 200–700 years. All maps are in the Antarctic Polar Stereographic projection (EPSG:3031), and panel a was prepared with Quantarctica (Matsuoka et al., 2021).

with larger SMB due to the increased vertical advection of cold snow which lowers the basal temperatures. On the other hand, considering very old ice near the bed, larger SMB increases the depth of the ice at a certain age and correspondingly reduces the age resolution of the ice (Dansgaard & Johnsen, 1969). SMB data sets commonly used in ice-sheet modeling (e.g., Huybrechts et al., 2000; Ritz et al., 2001; Van Liefferinge & Pattyn, 2013) tend to show overestimation in the East Antarctic inland around Dome Fuji (e.g., Fujita et al., 2011; Satow et al., 1999), which can lead to underestimation of basal melting as indicated by a simulation study where observed SMB was partially implemented (Saito & Abe-Ouchi, 2004). Better areal coverage of reliable field-based SMB data for integration into ice-sheet models is thus critical for searching Oldest Ice in the candidate areas.

Here, we present SMB over the last three centuries in the vicinity of Dome Fuji based on microwave radar profiling and shallow firn coring. High local SMB variability at scales of a few hundred meters is quantified and related to local surface slopes. We further discuss the results in context of ice-sheet mass balance and the presence of Oldest Ice.

2. Dome Fuji Region

As a part of a site survey for future deep ice coring of Oldest Ice (Text S1), we investigated the area (Figure 1) south of Dome Fuji Station where two deep ice cores were drilled earlier (Kawamura et al., 2007, 2017; Watanabe et al., 2003). This area includes the current topographic crest, constituting a major continental drainage boundary. Satellite microwave emission data indicate a distinct contrast in SMB across the crest (Fujita et al., 2011). At Dome Fuji Station near the crest, SMB has been estimated to 25.5 ± 0.3 kg m^{-2} a^{-1} averaged over 1260–2001 CE (Igarashi et al., 2011), and 28 ± 3 kg m^{-2} a^{-1} over the early Holocene (Svensson et al., 2015). For a more recent period between 1995 and 2006, SMB was measured to be 27.3 ± 0.4 kg m^{-2} a^{-1} using multiple snow stakes near the station (Fujita et al., 2011; Kameda et al., 2008).

Larger-scale SMB data in the region have previously been collected from a long-term snow-stake network along the ~1,000 km traverse route from the coast to Dome Fuji Station (Hoshina et al., 2016), as well as using radar data and firn cores of scientific traverses of Japan-Sweden (Fujita et al., 2011) and Norway-US (Müller et al., 2010) during the 2007–2008 International Polar Year (Figure 1b). Fujita et al. (2011) showed that SMB varies between 24 and 30 kg m^{-2} a^{-1} over the past seven centuries along the northwestern divide within 400 km from Dome Fuji Station. Müller et al. (2010) showed that SMB averaged over the past 200 years ranges between 20 and 30 kg m^{-2} a^{-1} about 200 km inland of the Dome Fuji Station. Interpolation between these SMB transects indicate a spatial contrast in SMB across the continental divide (Figure 1b) which is broadly consistent with satellite microwave emission data (Fujita et al., 2011); see also Text S2.

Our new radar data coupled with multiple shallow firn cores give a uniquely dense sample of recent SMB over a large area, useful for assessing the impact of local variability on regional-scale SMB and for delineation of Oldest Ice.

3. Data and Methods

We surveyed the Dome Fuji region in the 2018–2019 austral summer with a new ultrawide-band FM-CW radar (Taylor et al., 2019) mounted on a platform of a tracked vehicle moving ~10 km/hr. The radar operates at 2–8-GHz with 6-GHz bandwidth, giving a depth resolution of about 25 mm in snow. After fast Fourier transform, coherent and incoherent averaging were performed to increase the signal-to-noise ratio. The processed data are spaced at ~1.1-m intervals over ~1,100 line kilometers in about 500 km^2 (Figure 1a). The study area was covered by a series of parallel profiles with a nominal separation of 1 km, and with numerous cross-over sites particularly near the survey camp and the firn core sites NDF and NDFN. In the radargram, we tracked the surface and three englacial reflectors, which were selected for their continuity across all profiles (Figure 2d). We assumed that the reflectors are isochrones that can be dated with depth chronology from firn cores.

Firn density-depth profiles are needed to determine reflector depths and SMB. Although SMB is spatially variable in our study area, the tracked reflectors are all in the shallow part of the firn (density <550 kg m^{-3}, Figure 2a) where densification is dominated by grain boundary sliding which is to first-order independent of SMB (Herron & Langway, 1980). This was confirmed by the similarity of the measured density-depth profiles in four firn cores drilled in the 2017–2018 and 2018–2019 seasons (Figure 2a). Density in the top several meters of firn is often underestimated due to the high variability in the near surface which creates irregularity in the sample volume of these fragile core segments (Weinhart et al., 2020). At 20-m depth, the cores are more stable and less error prone. We used a single linear fit between the average density down to ~1-m depth from multiple snow pit observations (Table S1) and the average density at ~20-m depth from the stable part of the cores (Table S2). To account for density measurement errors, we developed uncertainty bounds from Monte Carlo simulations (Text S3). The resulting linear function is $\rho = (9.11 \pm 1.27)d + (331 \pm 24.2)$ where ρ is the density (kg m^{-3}) and d is the depth (m). We also attempted various linear and polynomial fits with all core data, but found that it had little impact on the resulting SMB.

We derived a depth-profile of permittivity (ϵ) based on the fitted density profile following Kovacs et al. (1995): $\epsilon = 0.021d + 1.60$. This equation for local permittivity is used to derive depth-variable propagation speed and then accurate depths of the reflectors. Separately, the dielectric permittivity of the NDFN firn core was measured at −30 C at frequencies over 15–20 GHz with a ~30-mm resolution from the surface to 15.0 m with an open resonator method (Fujita et al., 2016). This resulted in a consistent permittivity profile of $\epsilon = 0.020d + 1.64$ (Figure 2c).

The radar reflectors were dated using data from the NDFN firn core that was drilled in the same season. There are nine independent radar profiles with 700 sampling points within 50 m from the NDFN core site. Within this zone, depths of the three tracked reflectors vary by 1.6–3.7% of their mean depths. Dielectric conductivity was measured along the core, revealing six peaks that were identified to be of volcanic origin and tied to sulfate peaks in the WAIS Divide ice core (Sigl et al., 2014), giving six aged depths in the top 20 m (Figure 2b and Table S3). We then constructed a depth-age model (Buizert et al., 2018) that assumes constant SMB between the volcanic tie points and accounts for uncertainties (2σ) due to tie-point matching, age interpolation, and firn density variability (Text S4). This resulted in reflector ages of 78.1 ± 4.5, 95.9 ± 4.1, and 263.7 ± 6.0 years before 2019 (Table S4).

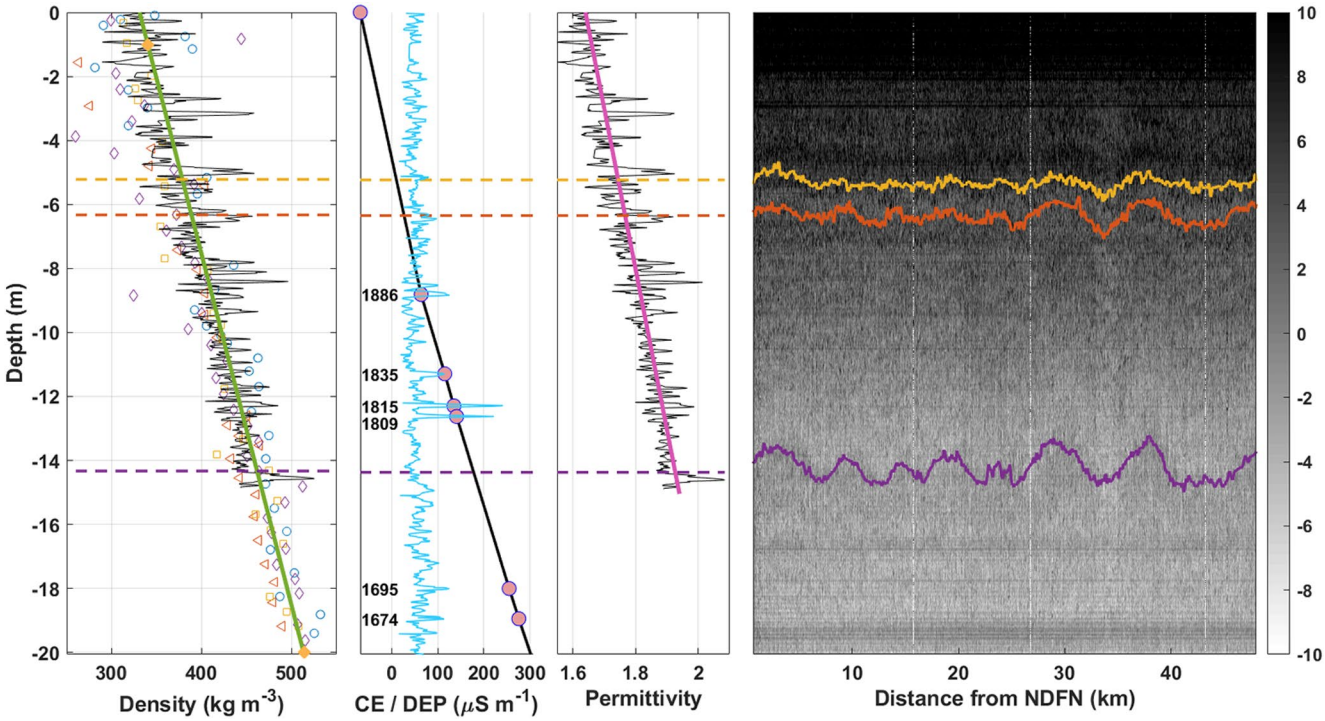

Figure 2. Radar and firn data. (a) Measured bulk density in the top 20 m of four shallow cores (colored open symbols) with locations shown in Figure 1a. A depth-density relationship (green line) was fitted to the spatially averaged densities down to ~1-m depth from snow pits and at ~20-m depth from firn cores (orange circles, Tables S1 and S2). The black curve shows density derived from permittivity (c) using Kovacs et al. (1995). (b) Chronology (CE) and dielectric conductivity (DEP) of the NDFN core. Six volcanic depth ages (pink markers) were used to construct a depth-age model (black line) to date the three tracked radar reflectors indicated with horizontal dashed lines. (c) Dielectric permittivity (ϵ) of the NDFN core with a linear fit (purple line). (d) Radargram between the NDFN site and Dome Fuji Station. The three tracked reflectors are highlighted; see Figure S1 for tracking procedures. The radargram shows returned power in dB relative to the mean value of the presented domain. See Figure 1a for profile location.

As a consistency check, we similarly derived reflector ages based on the NDF core that was drilled 1 year earlier at a location ~6 km south of NDFN (Table S5).

The nominal ice thickness of the surveyed region is around 2.5 km (Karlsson et al., 2018), so all tracked reflectors are within 0.6% of the ice thickness from the upper surface. Within this depth range, the depths of reflectors are mainly dependent on SMB. First-order densification processes are also accounted for in our analysis since both density and propagation speed are considered as depth variable. Therefore, SMB can be derived as the integrated mass from the surface to the three reflectors divided by the corresponding number of years, resulting in three reference SMB periods denoted T1 (1941–2019), T2 (1923–2019), and T3 (1755–2019).

4. Results

Observed spatial SMB patterns for the three periods are very similar (Figures 3, S2, and S3), and SMB uncertainties (2σ) somewhat decrease with depth: ±17.5% for T1, ±17.1% for T2, and ±14.8% for T3 (Text S5). To estimate regional-mean SMB values with highly variable data distributions, we first calculated the mean SMB in a 200 m × 200 m grid where data are available and then took the mean of the gridded SMB values. The regional-mean SMB obtained are 25.1 ± 4.4 (T1), 24.7 ± 4.2 (T2), and 22.5 ± 3.3 (T3) kg m^{-2} a^{-1}. The mean SMB values around the NDFN core site (200 m × 200 m) are 23.8 ± 4.2 (T1), 23.9 ± 4.1 (T2), and 21.6 ± 3.2 (T3) kg m^{-2} a^{-1}. While the comparable SMB derived from the core data is 24.4 ± 3.5 at T1 and T2, because of the linearity in the density-depth and age-depth models and 23.1 ± 3.0 kg m^{-2} a^{-1} at T3 (Table S4).

In our survey area, SMB is highest in the dome summit area within 20 km from Dome Fuji Station, and then gradually decreases downslope toward NDFN (Figure 3). SMB within the grid areas is more variable over short distances than the two segments to the Dome Fuji Station. We attribute this difference to surface slope (Figure 3).

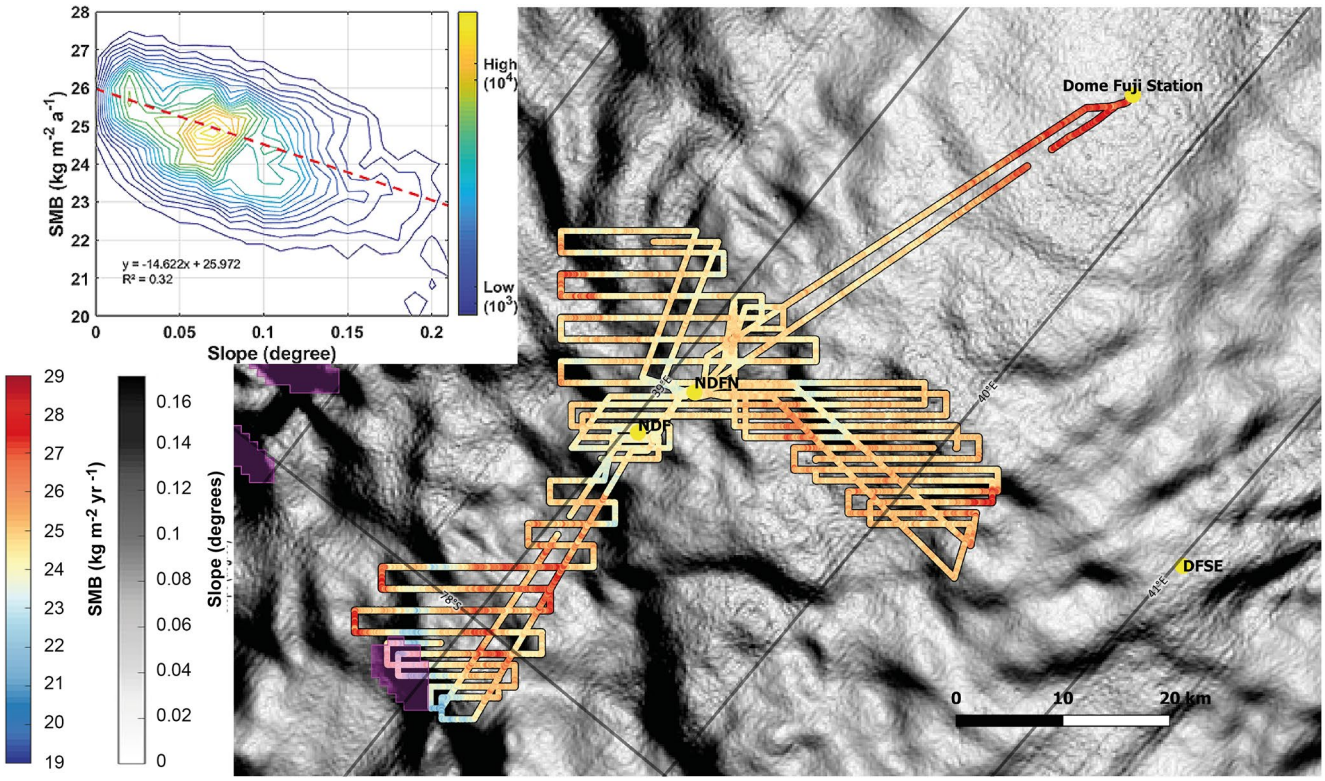

Figure 3. Profiles of surface mass balance (SMB) for the T2 period (1923–2019) plotted over surface slopes at 200-m resolution derived from the Reference Elevation Model of Antarctica (REMA; Howat et al., 2019). Satellite-derived wind scour areas are shown with light purple polygons (Das et al., 2013). Firn core sites are shown with yellow circles. Similar plots for the periods T1 and T3 are provided in Figures S2 and S3, respectively. The inset shows the relationship between SMB and REMA surface slopes for ∼1 million locations for the same period. The number of data points is shown using contours. The dashed red line shows the linear fit to the data.

We derived absolute magnitudes of surface slope for 200 m × 200 m grid cells using the Reference Elevation Model of Antarctica (REMA, Howat et al., 2019). The region between Dome Fuji Station and NDFN has small surface slopes (<0.03°) and there are no strong slope patterns. In contrast, the grid areas have more variable slopes, up to >0.12°, and distinct alternations of steeper slopes and flatter slopes. We observe larger SMB over flatter slopes and smaller SMB over steeper slopes. This relationship is robust even if slopes are calculated over shorter or longer distances. However, the correlation weakens when slopes are calculated over distances shorter than ∼100 m or distances longer than ∼2 km. Potential directional dependencies cannot be easily addressed as almost all observations are in southerly aspects.

We validated the gridded REMA slopes with independent surface slopes derived from ICESat-2 laser altimetry data. We used the ATL06 product (Smith et al., 2019) which has a surface elevation precision better than 9 cm on the Antarctic plateau (Brunt et al., 2019). Surface slopes are provided at a scale of 40 m along-track and 90 m across-track, and we further applied a running mean filter over 200-m distances along each laser beam before calculating absolute slopes comparable to REMA. The REMA and ICESat-2 slope patterns match very well (Figure S4b), and their mean and third quartile differences in slope magnitudes are 0.019° and 0.027°. Most larger discrepancies are associated with a few ICESat-2 ground tracks (Figure S5).

We quantified the observed SMB dependency on surface slopes derived from REMA using all ∼1 million data points (Figure 3 inset). We approximated this relationship linearly, $y = ax + b$, where x is the surface slope in degrees and y is measured SMB (kg m^{-2} a^{-1}), and obtained $(a, b, R^2) = (-11.4, 26.1, 0.22)$ for T1, $= (-14.6, 26.0, 0.32)$ for T2, and $= (-12.4, 23.6, 0.35)$ for T3. The results are consistent when using ICESat-2 data for surface slopes (Figure S5) or when calculating surface slopes at different length scales from ∼100 m to ∼2 km.

5. Discussion

Microwave radar layering has been used to measure recent SMB at various locations in Antarctica. However, most of earlier work has been done in West Antarctica, which has an order of magnitude larger SMB than the inland East Antarctica (Medley et al., 2013, 2015). The inland East Antarctic plateau has very low SMB and strong vertical vapor transportation near the surface resulting in depth hoar formation (Gallet et al., 2014; Scambos et al., 2012) which can be a challenge for SMB applications of microwave radar. Our study demonstrates that microwave radar can be used to determine spatial patterns of SMB in a low-accumulation region with abundant depth hoar.

Shallow radar reflectors are widely considered as isochrones in Greenland and West Antarctica (e.g., Spikes et al., 2004), but not yet well validated in the inland East Antarctic plateau. The separately analyzed NDF core is used for this validation and to examine our age uncertainties (2σ) derived from the NDFN core. The NDF core location is ~6 km south of NDFN and 330 m away from one radar profile. There are 663 data points within 350 m from the core site. After correcting for the 1 year difference between the radar survey and the NDF coring, averaged depths of L1, L2, and L3 reflectors within 330–350 m from the core site are 80.0 ± 3.6, 98.7 ± 3.3, and 256.7 ± 3.4 years before 2019, respectively. These age estimates are all within 3% of the reference ones derived from the NDFN core, and the associated uncertainties are overlapping (Tables S4 and S5).

This dense radar survey grid combined with multiple firn cores (Figure 1) give us an opportunity to estimate area-averaged SMB with high confidence over the past three centuries. The regional-mean SMB for each of the three periods appears to slightly increase with time from 22.5 to 25.1 kg m^{-2} a^{-1} which is consistent with many other locations on the Antarctic plateau (Fujita et al., 2011); however, given the estimated SMB uncertainty this trend is not statistically robust. As inferred from past radar traverse data (Figure 1b), larger-scale SMB shows a slight decrease from Dome Fuji Station toward the southern end of our study area (Figure S6). Our regional-mean SMB values are within the range of the estimates from two commonly used regional climate models: 22.5 kg m^{-2} a^{-1} (van Wessem et al., 2018) and 31 kg m^{-2} a^{-1} (Agosta et al., 2019). We observed the lowest SMB in a wind scour zone (Figure 3), a steep eroded surface feature formed by wind acceleration and probably related to the bed topography (Das et al., 2013). Topographically induced snow redistribution and sublimation by downslope wind is a likely mechanism to explain the observed SMB variability in our study area.

Previous studies have also pointed out correspondences between SMB and surface slope, as well as between surface and bed slopes (Black & Budd, 1964; Cavitte et al., 2018; Frezzotti et al., 2004, 2005, 2007; Fujita et al., 2002, 2011; Furukawa et al., 1996; Le Meur et al., 2018; Minghu et al., 2011; Wang et al., 2015). However, these studies relied on along-track slopes derived using GPS data along the radar transect or digital elevation models (DEM) with spatial resolutions at kilometer scales. The surface elevation products of REMA with a native 8-m horizontal resolution allows us to derive precise slopes at higher resolutions (Figure 4), which we have validated with independent analysis of ICESat-2 altimetry data (Figure S5). Our analysis shows that SMB can differ by 30% within ~500 km^2 in the vicinity of an inland dome where wind is particularly weak, and where SMB is typically assumed to be nearly uniform.

We used the new SMB data to re-evaluate promising Oldest Ice locations proposed earlier (Karlsson et al., 2018; Van Liefferinge et al., 2018). Their studies assumed regional-mean SMB values (van de Berg et al., 2006) that are 15–60% larger than our new estimate south of Dome Fuji, which is consistent with the previous observation at Dome Fuji Station. The first guiding principle to search for Oldest Ice is frozen bed conditions (Fischer et al., 2013). The threshold (maximum) geothermal heat flow to maintain a frozen bed over the last 1.5 million years becomes ~10 mW m^{-2} lower when the new SMB data are applied. Van Liefferinge et al. (2018) diagnosed ~25% of the Dome Fuji region (Figure 3 domain) as promising Oldest Ice sites. However, if SMB is assumed uniform at the regional-mean SMB from our observations, then the areal fraction of the promising sites would be 5–18% of Figure 3 domain, depending on the data set used for geothermal heat flow. This areal fraction is also sensitive to ice thickness, and the estimate above was made using a regional ice thickness data set (Karlsson et al., 2018). The results confirm the importance of using observational SMB for investigating the thermal condition and age of the deep ice (Saito & Abe-Ouchi, 2004).

We explored possible impacts of the SMB-slope relationship on estimating large-scale SMB over inland East Antarctica using our simple parametrization of SMB with local slopes (Figure S6), though SMB depends on many other factors including the curvature of the surface. Regional climate models typically have grid-cell sizes of a few tens of kilometers, and thus slopes over these cells are very low (10^{-2}–10^{-5} degrees) compared to surface slopes at the scale of a few hundred meters (up to 10^{-1}–10^{-2} degrees, Figure S4a). For a relative estimate of

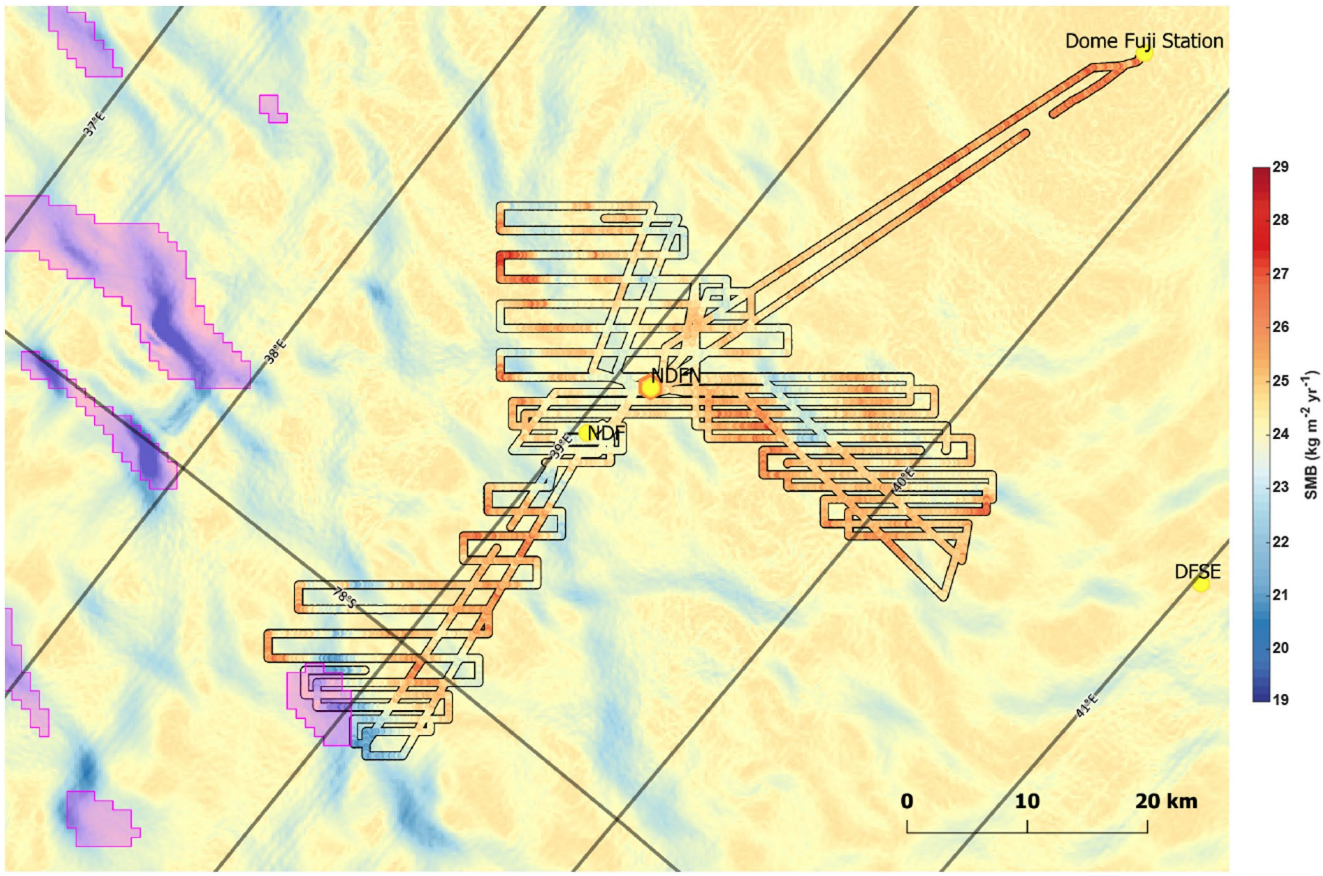

Figure 4. A map of surface mass balance (SMB) estimate derived from our slope relationship for the T2 period ($y = 14.6x + 26.0$). Radar-derived SMB estimates for the T2 period are shown along the radar transects using the same colorbar. Satellite-derived wind scour areas are also shown with light purple polygons (Das et al., 2013).

topographic SMB impacts, we first derived surface slopes using REMA at 200-m resolution for the entire East Antarctic plateau. Second, REMA was downsampled to generate a coarser DEM with 25-km resolution, which is comparable to those used in regional climate models. Third, slopes derived from the coarse DEM were subtracted from the slopes derived from REMA at 200-m resolution to determine the residual slope variability. By applying the SMB-slope parametrization for the T2 period for the residual slopes across the plateau, we infer a widespread occurrence of low-SMB zones related to local slope variability (Figure S6). If the slope-induced residual SMB is integrated over the ice-sheet interior, we obtain total numbers of 13.0 Gt a^{-1} for areas higher than 3 km a.s.l. and 3.6 Gt a^{-1} for areas higher than 3.5 km a.s.l. This corresponds to 8–10% of the integrated SMB of regional climate models over the same areas (e.g., van Wessem et al., 2018). This could imply an overestimation of ice-sheet SMB in larger-scale SMB products, or it could be balanced by an opposite offset over flatter slopes. Our parameterization is only based on the observed SMB conditions near the inland dome, and effects of wind on SMB can be stronger over katabatic wind regions, which may cause an even larger slope dependency on SMB. More extensive SMB measurements are needed to accurately quantify SMB over large areas, and ultrawide-band microwave radar is the most practical method for such missions.

6. Conclusions

SMB over the past three centuries was mapped using microwave radar reflectors in the top 15 m of the firn over a 500 km^2 area near Dome Fuji in East Antarctica. Our dense survey grid enabled us to precisely evaluate regional-mean SMB and document small-scale SMB variations. The regional-mean SMB for the past 264 ± 6 years was quantified to 22.5 ± 3.3 kg m^{-2} a^{-1}, which is considerably lower than what was used to delineate promising Oldest Ice in earlier studies. With an updated SMB, the areal fraction of promising sites in the Dome Fuji region

is reduced significantly, and a further refined estimate using the spatial SMB, ice thickness, and geothermal heat flow is needed. Our SMB observations reveal a ∼30% local variability and a strong negative correlation with surface slope at length scales from ∼100 m to ∼2 km. Using the high-resolution REMA product, we quantified for the first time the SMB-slope relationship at scales of a few hundred meters. If this relationship is generally valid in inland East Antarctica at elevations higher than 3 and 3.5 km a.s.l., then the local SMB anomalies associated with small-scale steeper slopes represent as much as 8–10% of the integrated SMB over the whole region. This is significant for assessments of Antarctica's overall mass balance and contribution to sea-level change.

Data Availability Statement

There are three data sets generated in this study: (a) Ice core data are archived at Arctic Data Archive System at National Institute of Polar Research https://doi.org/10.17592/001.2021102101. (b) Microwave radar data used for this work (version 1) are archived at University of Alabama Institutional Repository https://doi.org/10.48707/e5ck-q886. (c) SMB, slopes, and associate reflector characteristics are archived at the Norwegian Polar Data Centre https://doi.org/10.21334/npolar.2021.72d5e781.

Acknowledgments
This work was supported by financial contributions from the National Institute of Polar Research and Norwegian Polar Institute as a collaborative project with The University of Alabama and the University of Kansas. The 59th Japanese Antarctic Research Expedition (JARE) led by N. Kizu and the 60th JARE led by M. Tsutsumi and N. Harada prepared the traverse and provided the largest field supports including six field personnel. The Japanese component was also supported by the MEXT and JSPS grants 17H06320, 17H06104, and 18H05294. Norway's contribution is a part of Beyond EPICA Oldest Ice (BE-OI) project, which has received funding from the European Union's Horizon 2020 research and innovation programme under grant Agreement No. 730528 (BE-OI CSA), enabled by additional supports from British Antarctic Survey, the Belgian Science Policy Office and the International Polar Foundation. The Norwegian component was also supported by the Research Council of Norway's FRINATEK Grant 315246. We acknowledge Bob Hawley and Tate Meehan for their constructive reviews. This is BE-OI contribution number 24.

References

Agosta, C., Amory, C., Kittel, C., Orsi, A., Favier, V., Gallée, H., & Fettweis, X. (2019). Estimation of the Antarctic surface mass balance using the regional climate model MAR (1979–2015) and identification of dominant processes. *The Cryosphere*, *13*(1), 281–296. https://doi.org/10.5194/tc-13-281-2019

Black, H., & Budd, W. (1964). Accumulation in the region of Wilkes, Wilkes Land, Antarctica. *Journal of Glaciology*, *5*(37), 3–14. https://doi.org/10.3189/s0022143000028549

Brunt, K. M., Neumann, T. A., & Smith, B. E. (2019). Assessment of ICESat-2 ice sheet surface heights, based on comparisons over the interior of the Antarctic ice sheet. *Geophysical Research Letters*, *46*, 13072–13078. https://doi.org/10.1029/2019GL084886

Buizert, C., Sigl, M., Severi, M., Markle, B. R., Wettstein, J. J., McConnell, J. R., & Steig, E. J. (2018). Abrupt ice-age shifts in southern westerly winds and Antarctic climate forced from the north. *Nature*, *563*(7733), 681. https://doi.org/10.1038/s41586-018-0727-5

Cavitte, M. G. P., Parrenin, F., Ritz, C., Young, D. A., Van Liefferinge, B., Blankenship, D. D., et al. (2018). Accumulation patterns around Dome C, East Antarctica, in the last 73 kyr. *The Cryosphere*, *12*(4), 1401–1414. https://doi.org/10.5194/tc-12-1401-2018

Dansgaard, W., & Johnsen, S. J. (1969). A flow model and a time scale for the ice core from Camp Century, Greenland. *Journal of Glaciology*, *8*(53), 215–223. https://doi.org/10.3189/s0022143000031208

Das, I., Bell, R. E., Scambos, T. A., Wolovick, M., Creyts, T. T., Studinger, M., et al. (2013). Influence of persistent wind scour on the surface mass balance of Antarctica. *Nature Geoscience*, *6*(5), 367–371. https://doi.org/10.1038/ngeo1766

Fischer, H., Severinghaus, J., Brook, E., Wolff, E., Albert, M., Alemany, O., et al. (2013). Where to find 1.5 million yr old ice for the IPICS "Oldest-Ice" ice core. *Climate of the Past*, *9*(6), 2489–2505. https://doi.org/10.5194/cp-9-2489-2013

Frezzotti, M., Pourchet, M., Flora, O., Gandolfi, S., Gay, M., Urbini, S., et al. (2004). New estimations of precipitation and surface sublimation in East Antarctica from snow accumulation measurements. *Climate Dynamics*, *23*(7–8), 803–813. https://doi.org/10.1007/s00382-004-0462-5

Frezzotti, M., Pourchet, M., Flora, O., Gandolfi, S., Gay, M., Urbini, S., et al. (2005). Spatial and temporal variability of snow accumulation in East Antarctica from traverse data. *Journal of Glaciology*, *51*(172), 113124. https://doi.org/10.3189/172756505781829502

Frezzotti, M., Urbini, S., Proposito, M., Scarchilli, C., & Gandolfi, S. (2007). Spatial and temporal variability of surface mass balance near Talos Dome, East Antarctica. *Journal of Geophysical Research*, *112*, F02032. https://doi.org/10.1029/2006JF000638

Fujita, S., Goto-Azuma, K., Hirabayashi, M., Hori, A., Iizuka, Y., Motizuki, Y., et al. (2016). Densification of layered firn in the ice sheet at Dome Fuji, Antarctica. *Journal of Glaciology*, *62*(231), 103–123. https://doi.org/10.1017/jog.2016.16

Fujita, S., Holmlund, P., Andersson, I., Brown, I., Enomoto, H., Fujii, Y., et al. (2011). Spatial and temporal variability of snow accumulation rate on the East Antarctic ice divide between Dome Fuji and EPICA DML. *The Cryosphere*, *5*(4), 1057–1081. https://doi.org/10.5194/tc-5-1057-2011

Fujita, S., Maeno, H., Furukawa, T., & Matsuoka, K. (2002). Scattering of VHF radio waves from within the top 700 m of the Antarctic ice sheet and its relation to the depositional environment: A case-study along the Syowa-Mizuho-Dome Fuji traverse. *Annals of Glaciology*, *34*, 157–164. https://doi.org/10.3189/172756402781817888

Furukawa, T., Kamiyama, K., & Maeno, H. (1996). Snow surface features along the traverse route from the coast to Dome Fuji Station, Queen Maud Land, Antarctica. *Proceedings of the NIPR Symposium on Polar Meteorology and Glaciology*, *10*, 13–24.

Gallet, J.-C., Domine, F., Savarino, J., Dumont, M., & Brun, E. (2014). The growth of sublimation crystals and surface hoar on the Antarctic plateau. *The Cryosphere*, *8*(4), 1205–1215. https://doi.org/10.5194/tc-8-1205-2014

Herron, M. M., & Langway, C. C. (1980). Firn densification: An empirical model. *Journal of Glaciology*, *25*(93), 373–385. https://doi.org/10.3189/S0022143000015239

Hoshina, Y., Fujita, K., Iizuka, Y., & Motoyama, H. (2016). Inconsistent relationships between major ions and water stable isotopes in Antarctic snow under different accumulation environments. *Polar Science*, *10*(1), 1–10. https://doi.org/10.1016/j.polar.2015.12.003

Howat, I. M., Porter, C., Smith, B. E., Noh, M.-J., & Morin, P. (2019). The Reference Elevation Model of Antarctica. *The Cryosphere*, *13*(2), 665–674. https://doi.org/10.5194/tc-13-665-2019

Huybrechts, P., Steinhage, D., Wilhelms, F., & Bamber, J. (2000). Balance velocities and measured properties of the Antarctic ice sheet from a new compilation of gridded data for modelling. *Annals of Glaciology*, *30*, 52–60. https://doi.org/10.3189/172756400781820778

Igarashi, M., Nakai, Y., Motizuki, Y., Takahashi, K., Motoyama, H., & Makishima, K. (2011). Dating of the Dome Fuji shallow ice core based on a record of volcanic eruptions from AD 1260 to AD 2001. *Polar Science*, *5*(4), 411–420. https://doi.org/10.1016/j.polar.2011.08.001

Jouzel, J., Masson-Delmotte, V., Cattani, O., Dreyfus, G., Falourd, S., Hoffmann, G., & Wolff, E. W. (2007). Orbital and millennial Antarctic climate variability over the past 800,000 years. *Science*, *317*(5839), 793–796. https://doi.org/10.1126/science.1141038

Kameda, T., Motoyama, H., Fujita, S., & Takahashi, S. (2008). Temporal and spatial variability of surface mass balance at Dome Fuji, East Antarctica, by the stake method from 1995 to 2006. *Journal of Glaciology*, *54*(184), 107–116. https://doi.org/10.3189/002214308784409062

Karlsson, N. B., Binder, T., Eagles, G., Helm, V., Pattyn, F., Van Liefferinge, B., & Eisen, O. (2018). Glaciological characteristics in the Dome Fuji region and new assessment for "oldest ice". *The Cryosphere*, *12*(7), 2413–2424. https://doi.org/10.5194/tc-12-2413-2018

Kawamura, K., Abe-Ouchi, A., Motoyama, H., Ageta, Y., Aoki, S., Azuma, N., & Yoshimoto, T. (2017). State dependence of climatic instability over the past 720,000 years from Antarctic ice cores and climate modeling. *Science Advances*, *3*(2), e1600446. https://doi.org/10.1126/sciadv.1600446

Kawamura, K., Parrenin, F., Lisiecki, L., Uemura, R., Vimeux, F., Severinghaus, J. P., et al. (2007). Northern hemisphere forcing of climatic cycles in Antarctica over the past 360,000 years. *Nature*, *448*(7156), 912–916. https://doi.org/10.1038/nature06015

Kovacs, A., Gow, A. J., & Morey, R. M. (1995). The in-situ dielectric constant of polar firn revisited. *Cold Regions Science and Technology*, *23*(3), 245–256. https://doi.org/10.1016/0165-232X(94)00016-Q

Le Meur, E., Magand, O., Arnaud, L., Fily, M., Frezzotti, M., Cavitte, M., & Urbini, S. (2018). Spatial and temporal distributions of surface mass balance between Concordia and Vostok stations, Antarctica, from combined radar and ice core data: First results and detailed error analysis. *The Cryosphere*, *12*(5), 1831–1850. https://doi.org/10.5194/tc-12-1831-2018

Matsuoka, K., Skoglund, A., Roth, G., de Pomereu, J., Griffiths, H., Headland, R., & Melvr, Y. (2021). Quantarctica, an integrated mapping environment for Antarctica, the Southern Ocean, and sub-Antarctic islands. *Environmental Modelling & Software*, *140*, 105015. https://doi.org/10.1016/j.envsoft.2021.105015

Medley, B., Joughin, I., Das, S. B., Steig, E. J., Conway, H., Gogineni, S., & Nicolas, J. P. (2013). Airborne-radar and ice-core observations of annual snow accumulation over Thwaites Glacier, West Antarctica confirm the spatiotemporal variability of global and regional atmospheric models. *Geophysical Research Letters*, *40*, 3649–3654. https://doi.org/10.1002/grl.50706

Medley, B., Ligtenberg, S. R. M., Joughin, I., Van den Broeke, M. R., Gogineni, S., & Nowicki, S. (2015). Antarctic firn compaction rates from repeat-track airborne radar data: I. Methods. *Annals of Glaciology*, *56*(70), 155–166. https://doi.org/10.3189/2015aog70a203

Minghu, D., Cunde, X., Yuansheng, L., Jiawen, R., Shugui, H., Bo, J., & Bo, S. (2011). Spatial variability of surface mass balance along a traverse route from Zhongshan station to Dome A, Antarctica. *Journal of Glaciology*, *57*(204), 658–666. https://doi.org/10.3189/002214311797409820

Mouginot, J., Scheuchl, B., & Rignot, E. (2017). MEaSUREs Antarctic boundaries for IPY 2007–2009 from satellite radar, Version 2 [Data set]. Boulder, Colorado USA. NASA National Snow and Ice Data Center Distributed Active Archive Center. https://doi.org/10.5067/AXE4121732AD

Müller, K., Sinisalo, A., Anschütz, H., Hamran, S.-E., Hagen, J.-O., McConnell, J. R., & Pasteris, D. R. (2010). An 860 km surface mass-balance profile on the East Antarctic plateau derived by GPR. *Annals of Glaciology*, *51*(55), 1–8. https://doi.org/10.3189/172756410791392718

Ritz, C., Rommelaere, V., & Dumas, C. (2001). Modeling the evolution of Antarctic ice sheet over the last 420,000 years: Implications for altitude changes in the Vostok region. *Journal of Geophysical Research: Atmospheres*, *106*(D23), 31943–31964. https://doi.org/10.1029/2001jd900232

Saito, F., & Abe-Ouchi, A. (2004). Thermal structure of Dome Fuji and east Dronning Maud Land, Antarctica, simulated by a three-dimensional ice-sheet model. *Annals of Glaciology*, *39*, 433–438. https://doi.org/10.3189/172756404781814258

Satow, K., Watanabe, O., Shoji, H., & Motoyama, H. (1999). The relationship among accumulation rate, stable isotope ratio and surface temperature on the plateau of east Dronning Maud Land, Antarctica. *Polar Meteorology and Glaciology*, *13*, 43–52.

Scambos, T. A., Frezzotti, M., Haran, T., Bohlander, J., Lenaerts, J. T. M., Van Den Broeke, M., et al. (2012). Extent of low-accumulation 'wind glaze' areas on the East Antarctic plateau: Implications for continental ice mass balance. *Journal of Glaciology*, *58*(210), 633–647. https://doi.org/10.3189/2012jog11j232

Sigl, M., McConnell, J. R., Toohey, M., Curran, M., Das, S. B., Edwards, R., et al. (2014). Insights from Antarctica on volcanic forcing during the common era. *Nature Climate Change*, *4*(8), 693–697. https://doi.org/10.1038/nclimate2293

Smith, B., Fricker, H. A., Holschuh, N., Gardner, A. S., Adusumilli, S., Brunt, K. M., et al. (2019). Land ice height-retrieval algorithm for NASA's ICESat-2 photon-counting laser altimeter. *Remote Sensing of Environment*, *233*, 111352. https://doi.org/10.1016/j.rse.2019.111352

Spikes, V. B., Hamilton, G. S., Arcone, S. A., Kaspari, S., & Mayewski, P. A. (2004). Variability in accumulation rates from GPR profiling on the west Antarctic Plateau. *Annals of Glaciology*, *39*, 238244. https://doi.org/10.3189/172756404781814393

Svensson, A., Fujita, S., Bigler, M., Braun, M., Dallmayr, R., Gkinis, V., & Vinther, B. M. (2015). On the occurrence of annual layers in Dome Fuji ice core early holocene ice. *Climate of the Past*, *11*(9), 1127–1137. https://doi.org/10.5194/cp-11-1127-2015

Taylor, R. A., Gogineni, S., Gurbuz, S., Kolpuke, S., Li, L., ONeill, C., et al. (2019). A prototype ultra-wideband FMCW radar for snow and soil-moisture measurements. In *2019 IEEE International Geoscience and Remote Sensing Symposium (IGARSS 2019)* (pp. 3974–3977). https://doi.org/10.1109/IGARSS.2019.8899024

van de Berg, W. J., van den Broeke, M. R., Reijmer, C. H., & van Meijgaard, E. (2006). Reassessment of the Antarctic surface mass balance using calibrated output of a regional atmospheric climate model. *Journal of Geophysical Research*, *111*(D11), https://doi.org/10.1029/2005jd006495

Van Liefferinge, B., & Pattyn, F. (2013). Using ice-flow models to evaluate potential sites of million year-old ice in Antarctica. *Climate of the Past*, *9*(5), 2335. https://doi.org/10.5194/cp-9-2335-2013

Van Liefferinge, B., Pattyn, F., Cavitte, M. G. P., Karlsson, N. B., Young, D. A., Sutter, J., & Eisen, O. (2018). Promising oldest ice sites in East Antarctica based on thermodynamical modelling. *The Cryosphere*, *12*(8), 2773–2787. https://doi.org/10.5194/tc-12-2773-2018

van Wessem, J. M., van de Berg, W. J., Noël, B. P. Y., van Meijgaard, E., Amory, C., Birnbaum, G., et al. (2018). Modelling the climate and surface mass balance of polar ice sheets using RACMO2—Part 2: Antarctica (1979–2016). *The Cryosphere*, *12*(4), 1479–1498. https://doi.org/10.5194/tc-12-1479-2018

Wang, Y., Hou, S., Sun, W., Lenaerts, J. T. M., van den Broeke, M. R., & van Wessem, J. M. (2015). Recent surface mass balance from Syowa Station to Dome F, East Antarctica: Comparison of field observations, atmospheric reanalyses, and a regional atmospheric climate model. *Climate Dynamics*, *45*(9–10), 2885–2899. https://doi.org/10.1007/s00382-015-2512-6

Watanabe, O., Jouzel, J., Johnsen, S., Parrenin, F., Shoji, H., & Yoshida, N. (2003). Homogeneous climate variability across East Antarctica over the past three glacial cycles. *Nature*, *422*, 509–512. https://doi.org/10.1038/nature01525

Weinhart, A. H., Freitag, J., Hörhold, M., Kipfstuhl, S., & Eisen, O. (2020). Representative surface snow density on the East Antarctic plateau. *The Cryosphere*, *14*(11), 3663–3685. https://doi.org/10.5194/tc-14-3663-2020

References From the Supporting Information

Adusumilli, S., Fish, M. A., Fricker, H. A., & Medley, B. (2021). Atmospheric river precipitation contributed to rapid increases in surface height of the west Antarctic ice sheet in 2019. *Geophysical Research Letters*, *48*, e2020GL091076. https://doi.org/10.1029/2020GL091076

Anschütz, H., Müller, K., Isaksson, E., McConnell, J. R., Fischer, H., Miller, H., & Winther, J.-G. (2009). Revisiting sites of the south pole Queen Maud Land traverses in East Antarctica: Accumulation data from shallow firn cores. *Journal of Geophysical Research*, *114*, D24106. https://doi.org/10.1029/2009JD012204

Birnbaum, G., Freitag, J., Brauner, R., König-Langlo, G., Schulz, E., Kipfstuhl, S., et al. (2010). Strong-wind events and their influence on the formation of snow dunes: Observations from Kohnen Station, Dronning Maud Land, Antarctica. *Journal of Glaciology*, *56*(199), 891–902. https://doi.org/10.3189/002214310794457272

Braaten, D. A. (2000). Direct measurements of episodic snow accumulation on the Antarctic polar plateau. *Journal of Geophysical Research: Atmospheres*, *105*(D8), 10119–10128. https://doi.org/10.1029/2000JD900099

Bromwich, D., Guo, Z., Bai, L., & Chen, Q. (2004). Modeled Antarctic precipitation. Part I: Spatial and temporal variability*. *Journal of Climate*, *17*(3), 427–447. https://doi.org/10.1175/1520-0442(2004)017<0427:mappis>2.0.co;2

Gorodetskaya, I. V., Tsukernik, M., Claes, K., Ralph, M. F., Neff, W. D., & Van Lipzig, N. P. M. (2014). The role of atmospheric rivers in anomalous snow accumulation in East Antarctica. *Geophysical Research Letters*, *41*, 6199–6206. https://doi.org/10.1002/2014GL060881

Noone, D., & Simmonds, I. (1998). Implications for the interpretation of ice-core isotope data from analysis of modelled Antarctic precipitation. *Annals of Glaciology*, *27*, 398–402. https://doi.org/10.3189/1998aog27-1-398-402

Reijmer, C. H., & Van Den Broeke, M. (2003). Temporal and spatial variability of the surface mass balance in Dronning Maud Land, Antarctica, as derived from automatic weather stations. *Journal of Glaciology*, *49*(167), 512–520. https://doi.org/10.3189/172756503781830494

Schlosser, E., Duda, M. G., Powers, J. G., & Manning, K. W. (2008). Precipitation regime of Dronning Maud Land, Antarctica, derived from Antarctic mesoscale prediction system (amps) archive data. *Journal of Geophysical Research*, *113*, D24108. https://doi.org/10.1029/2008JD009968

Schlosser, E., Manning, K. W., Powers, J. G., Duda, M. G., Birnbaum, G., & Fujita, K. (2010). Characteristics of high-precipitation events in Dronning Maud Land, Antarctica. *Journal of Geophysical Research*, *115*, D14107. https://doi.org/10.1029/2009JD013410

Van Den Broeke, M. R., Reijmer, C. H., & Van De Wal, R. S. W. (2004). A study of the surface mass balance in Dronning Maud Land, Antarctica, using automatic weather stations. *Journal of Glaciology*, *50*(171), 565–582. https://doi.org/10.3189/172756504781829756